Icarus **140**, 92–105 (1999)
Article ID icar.1999.6113, available online at http://www.idealibrary.com on

The Ionosphere of Titan: Ideal Diurnal and Nocturnal Cases

Marina Galand

HAO-NCAR, P.O. Box 3000, Boulder, Colorado 80307-3000
E-mail: galand@ucar.edu

Jean Lilensten

LIS-ENSIEG, BP 46, 38 402 St. Martin d'Hères cedex, France

Dominique Toublanc

CESR, 9 Av. du Colonel Roche, 31029 Toulouse cedex 04, France

and

Sylvestre Maurice

Observatoire Midi-Pyrénées, 14 Av. Ed. Belin, 31400 Toulouse, France

Received February 17, 1998; revised January 28, 1999

We have solved a stationary Boltzmann transport equation to describe the ionosphere of Titan in two simple cases. The first one deals with the satellite being outside the Kronian magnetosphere on the dayside of Saturn, which happens under strong solar wind conditions. In that case, the main energy source of ionization is the solar photons. We show the effect of the photoionization and the secondary ion production for a solar zenith angle of 45°. The electron production peaks at 25 electrons s^{-1} cm^{-3} around 1000 km. We estimate the electron density from a comprehensive chemical code. This electron density is then compared with the one computed from a simple recombination model. Finally, we determine the intensity of nitrogen emissions, which are compared to the Voyager 1 measurements.

In the second case, the satellite is inside Saturn's magnetosphere. We show the effect of the ionization due to electron precipitation at night, above the polar regions. The input electron flux is measured by the Voyager probes, gathered from several instruments on board. A simple Kappa distribution is given to model a mean electron flux precipitating on Titan. We show that the electron production ranges between 1 to 5 electrons s^{-1} cm^{-3} between about 550 and 650 km. The electron production due to the photoionization above the pole is evaluated and compared to the effect of the kronian electron precipitation.

Key Words: **ionosphere; photochemistry; photometry; satellite of Saturn; Titan (atmosphere).**

1. INTRODUCTION

The atmosphere of Titan is mainly composed of nitrogen, like Earth's. The NASA/ESA Cassini spacecraft was launched in 1997 with a primary objective of studying Titan's environment; in support of this mission, it is necessary to develop a model of Titan's ionosphere. Earth's modelers are fairly well equipped for such a study. Many tools have been developed, that solve transport, continuity, momentum, and energy equations. However, the magnetic conditions are drastically different in Titan's and Earth's environments: Earth's magnetic field lines act as a natural guide to drive the ionized particles. On the other hand, Titan is presumably not magnetized, but orbits around Saturn, which is a magnetized planet. Different cases are possible (Wolf and Neubauer 1982): Titan may be outside the Kronian magnetosphere when the solar wind pressure compresses the magnetopause inside 20 Saturn radii; or it may be fully immersed within the magnetosphere of Saturn.

Among these situations, we present two cases of special interest for Titan's ionosphere. The first case deals with the satellite being outside the Kronian magnetosphere and with the photons as the only source of ionization. The solar wind is not taken into account: the density of the solar wind at Titan is only 0.05 particle per cubic centimeter. The effect of the solar electrons and protons on Titan's ionosphere is therefore expected to be much smaller than the effect of the solar photon flux and is neglected in this study. We perform our computation near the equator for a solar zenith angle of 45°. The second case deals with Titan being within Saturn's magnetosphere, without photoionization due to the solar photons. Titan has a diurnal rotation period of 16 days, equal to its period around Saturn, so that part of the satellite is always at night for several days. The particle precipitations originating in the magnetosphere of Saturn are an effective source of energy upon Titan's darkside atmosphere, as attested by Voyager

0019-1035/99 $30.00

emission observations (Hall *et al.* 1992). The single energy source we consider for the nocturnal case is the magnetospheric electron precipitation. Moreover, we perform our computation at the polar regions, where a simple magnetic model is adopted.

For these two extreme cases, we study the degradation of an energetic flux interacting with Titan's atmosphere; this flux is either the EUV solar flux or the Kronian electron precipitation. The Boltzmann transport equation is solved providing the stationary electron flux in altitude, energy, and angle. Then we deduce parameters such as the ion and electron productions and the excitation rates for each constituent of the atmosphere. Using a comprehensive chemical model, we also determine the electron and ion densities.

The transport of electrons in Titan's ionosphere has already been studied by Gan *et al*. (1992) and Keller *et al*. (1992, 1994). In addition to the electron transport equation, they have solved the electron energy equation and used a photochemical ionospheric model (Keller *et al*. 1992) which gives access to the characteristics of the thermal population. Moreover, Keller *et al*. (1994) have included MHD effects for the ramside of Titan, the satellite being located within the Kronian magnetosphere. They have evaluated the effect of the different energy sources in the ionosphere of Titan, with the Kronian magnetic field lines draped around Titan. The originality of the present study is that, using a similar approach (although the energetic electron transport code is here based on a multistream method (Lummerzheim *et al*. 1989)), we propose a simple recombination coefficient to retrieve the dayside electron density from the electron production, allowing modelers to get a rough idea of the electron density from the computation of the production. In the nightside, we propose an incident Kronian electron flux based on Voyager particle measurements from different instruments. The gathering of these different experiments makes it possible to draw an experimental spectrum and to study its influence on Titan's ionosphere.

The transport equation at Titan is presented in Section 2. The first case illustrating the dayside configuration is described in Section 3. First, the electron and ion production rates are proposed and compared. Then we present the results of a chemical scheme which computes the ion and electron densities from the production. The electron density computed with this model is then compared with a density computed with the effective recombination coefficient method, and a coefficient is proposed that allows a fast estimate of the electron density from the electron production. Moreover, from the computed electron flux we deduce the intensity of different nitrogen emissions and compare them with Voyager 1 observations. The results obtained in the second case dealing with the nocturnal configuration is presented in Section 4. We propose a model of the suprathermal electron precipitation, based on a detailed analysis of Voyager particle measurements. In Section 5, the different results are summarized and discussed; the electron production due to the photoionization above the pole is evaluated, too, and compared to the effect of the Kronian electron precipitations.

2. THE TRANSPORT MODEL AT TITAN

The transport equation has been detailed in several papers on Earth's ionosphere (Oran and Strickland 1978, Stamnes and Rees 1983). A brief theoretical background is proposed in this Section. The EUV solar flux (<102.7 nm) produces electrons by ionization of neutral particles. These photoelectrons with energies smaller than 248 eV, as well as the suprathermal precipitated electrons of the Kronian magnetosphere, are called "primary" electrons; they collide with the ambient atmosphere, producing heating, excitation, and ionization. That last reaction leads to the production of "secondary" electrons. The transport equation that describes the production of electrons governs a steady-state electron flux in the ionosphere. On Earth, the transport of the electrons is predominantly along the magnetic field lines. That physical constraint allows us to consider axial symmetry around the field line and simplifies the solution of the equation. Such a symmetry can be applied also at Titan. In the diurnal case, since the atmosphere is locally plane, horizontally stratified and since the primary photoproduction is isotropic, we assume that the particle flux is locally independent of the horizontal coordinates. Therefore the plane parallel symmetry is valid about the vertical direction. The z axis is vertical and the term "angle" refers to the one between the particle velocity and the vertical direction. In the nocturnal case, the Kronian magnetic lines penetrate Titan's ionosphere, at least at the polar regions (see Section 4), and the plane parallel symmetry is valid around these lines. Thus the z axis is directed along the Kronian magnetic lines and the term "angle" refers to the pitch angle. With the plane parallel symmetry, the transport equation can be written (Oran and Strickland 1978):

$$\begin{aligned}\mu \frac{\partial \Phi(\tau, E, \mu)}{\partial \tau(z, E)} &= -\Phi(\tau, E, \mu) + S(\tau, E, \mu) \\ &\quad + \frac{n_e(z)}{\sum_k n_k(z)\sigma_k^T(E)} \frac{\partial (L(E)\Phi(\tau, E, \mu))}{\partial E} \\ &\quad + \sum_l \frac{n_l(z)\sigma_l^T(E)}{\sum_k n_k(z)\sigma_k^T(E)} \int_{-1}^{+1} d\mu' \\ &\quad \times \int_E^{E_{\max}} dE' R_l(E', \mu' \to E, \mu)\Phi(\tau, E', \mu') \qquad (1)\end{aligned}$$

$\Phi(\tau, E, \mu)$ = stationary electron flux ($\mathrm{cm^{-2}\ s^{-1}\ eV^{-1}\ sr^{-1}}$)
z = altitude
$\tau(z, E)$ = electron scattering depth
E, E' = energies (eV) of scattered and incident electrons
μ, μ' = cosines of scattered and incident electron angles
R_l = redistribution function describing the degradation from a state (E', μ') to a state (E, μ) for the neutral species l
$\sigma_k^T(E)$ = total elastic and inelastic collision cross section for the neutral species k colliding with one electron at energy E

$n_k(z)$ = density of the neutral species k
$n_e(z)$ = electron density at altitude z.

The second term on the right-hand side of (1) is the primary photoelectron source (in units of cm^{-2} s^{-1} eV^{-1} sr^{-1}) caused by the solar EUV (when taken into account),

$$S(\tau, E, \mu) = \frac{1}{4\pi \sum_k n_k(z)\sigma_k^T(E)} \sum_{k,i} q_{k,i}(z, E), \qquad (2)$$

with the primary photoelectron production (cm^{-3} s^{-1} eV^{-1}) equal to

$$q_{k,i}(z, E) = n_k(z)\omega_{k,i}^{\text{ion}}(E_{h\nu})F_\infty(E_{h\nu}) \times \exp\left\{-\sum_m \omega_m^T(E_{h\nu})Ch(\chi)\int_z^{+\infty} n_m(z')\,dz'\right\}, \qquad (3)$$

$E = E_{h\nu} - I_{k,i}$, where $I_{k,i}$ is the ionization threshold for species k, state i, and $E_{h\nu}$ is the energy of the incident photon (corresponding to a UV line wavelength).
$\omega_{k,i}^{\text{ion}}(E_{h\nu})$ = photoionization cross section for species k, state i, written ω in order to avoid any confusion with the collision cross sections.
$F_\infty(E_{h\nu})$ = solar flux on the top of the ionosphere at energy $E_{h\nu}$, in photons cm^{-2} s^{-1} eV^{-1}.
$\omega_m^T(E_{h\nu})$ = photon absorption cross section of the neutral species m.

To obtain the primary production along a vertical column, a Chapman function $Ch(\chi)$ is used, as a function of the solar zenith angle χ (Rees 1989). Indeed, the photon beam can cross a large region in longitude and the curvature of the satellite has then to be considered.

The third term on the right side of (1) represents the losses due to frictional processes (collisions between photoelectrons or precipitated electrons and thermal electrons). The stopping cross section L is a function of E as well as of the ambient electron density, as described in Oran and Strickland (1978). Frictional processes become important at low energies (less than the ionization threshold) and do not influence the secondary electron production. The last term represents the electron production due to degradation of higher-energy fluxes through collisions between suprathermal electrons and neutral particles (Mantas 1973, Oran and Strickland 1978, Stamnes 1981). R_l is defined as the ratio of the sum of differential cross sections (sum over the different reactions (inelastic and elastic) between the electrons and neutrals) to the total cross section σ_l^T (Lummerzheim and Lilensten 1994, and references therein).

The primary photoelectron production can be found by integrating $q_{k,i}$ in energy:

$$P_p(z) = \sum_{k,i} \int q_{k,i}(z, E)\,dE. \qquad (4)$$

The secondary electron production is deduced from (1) as

$$P_s(z) = \sum_m n_m(z)\, 2\pi \int_{-1}^{+1} d\mu \int_{E_{\min}}^{E_{\max}} dE\,\sigma_m^{\text{ion}}(E)\Phi(z, E, \mu), \qquad (5)$$

$\sigma_m^{\text{ion}}(E)$ being the ionization collision cross section for species m.

The programs solving (1) and (3) are described in Lummerzheim and Lilensten (1994) and Lilensten *et al*. (1989) and will therefore not be redescribed here. The transport scheme is in a multistream discrete ordinate. It was first developed for terrestrial studies and widely tested versus experiments and other models. One of the tests is based on a comparison with a laboratory experiment. In 1976, Barrett and Hays shot beams of electrons at collimated energies through a box filled with N_2. A photometer analyzed the intensity of the N_2^+ 1N emissions all along the box. We could reproduce this emission with the kinetic code with an accuracy of better than 5% (Lummerzheim and Lilensten 1994). Another test consisted of using the stationary electron flux to compute a plasma line frequency from 80 to 300 km, which could fit the measured plasma line. The results were satisfying both at night and during the day (Nilsson *et al*. 1996). More recently, we used this code coupled with a fluid one including a chemical scheme to compute the electron density in Earth's ionosphere. The results were successfully compared to incoherent scatter radar measurements, for daytime conditions as well as nighttime conditions during electron precipitation events (Blelly *et al*. 1996). Finally, we could also reproduce a statistical model of ionospheric conductivities based on three years of measurements (Lilensten *et al*. 1996).

We only recently adapted this code to Titan's ionosphere. To do so, the parameters to change are the neutral atmosphere, the absorption and collision cross sections, the magnetic field model, and the solar photon input flux. The neutral atmosphere used here is the Yelle model (Yelle *et al*. 1997) including some argon. This model is shown in Fig. 1. The N_2 and CH_4 densities are the same as proposed by Fox and Yelle (1997). The exospheric temperature is 175 K. We performed our computations from 600 km (where the N_2 density is about 7.4×10^{12} cm^{-3}) to 1600 km. The photon absorption cross sections are shown in Fig. 2. The set comes from Torr and Torr (1985) and Fennelly and Torr (1992) for N_2, from Samson *et al*. (1989) for CH_4 and from Berkowitz (1979) and Marr and West (1976) for Ar. The set of collision cross section for N_2 is detailed in Lummerzheim and Lilensten (1994) and includes 12 excitation states. It comes from Davies *et al*. (1989) for CH_4 (with 6 excitation states) and from a very complete set including 49 excitation states for Ar, provided by Bretagne *et al*. (1986). Elastic and total inelastic (excitations plus ionization) cross sections between electrons and neutral species are plotted in Fig. 3. The ion species considered are N_2^+, CH_4^+, and Ar^+ produced through simple ionization of N_2, CH_4, and Ar, respectively; N^+ and CH_3^+ are obtained through dissociative ionizations and Ar^{2+} through double ionization.

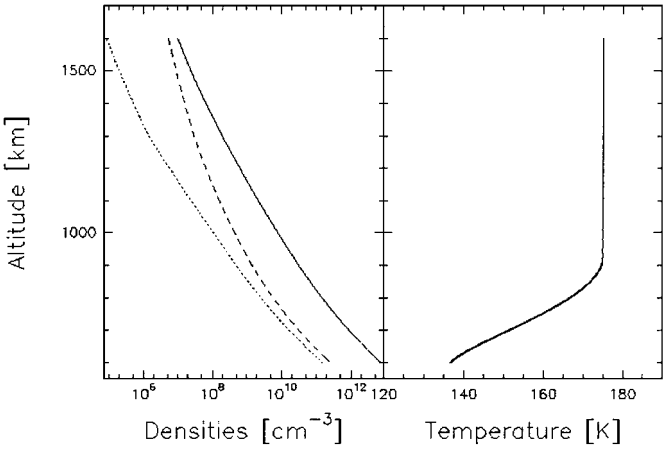

FIG. 1. Density height profiles (left) for N_2 (right curve), CH_4 (middle curve), and Ar (left curve) and neutral temperature height profile (right) in Titan's upper atmosphere (Yelle *et al*. 1997).

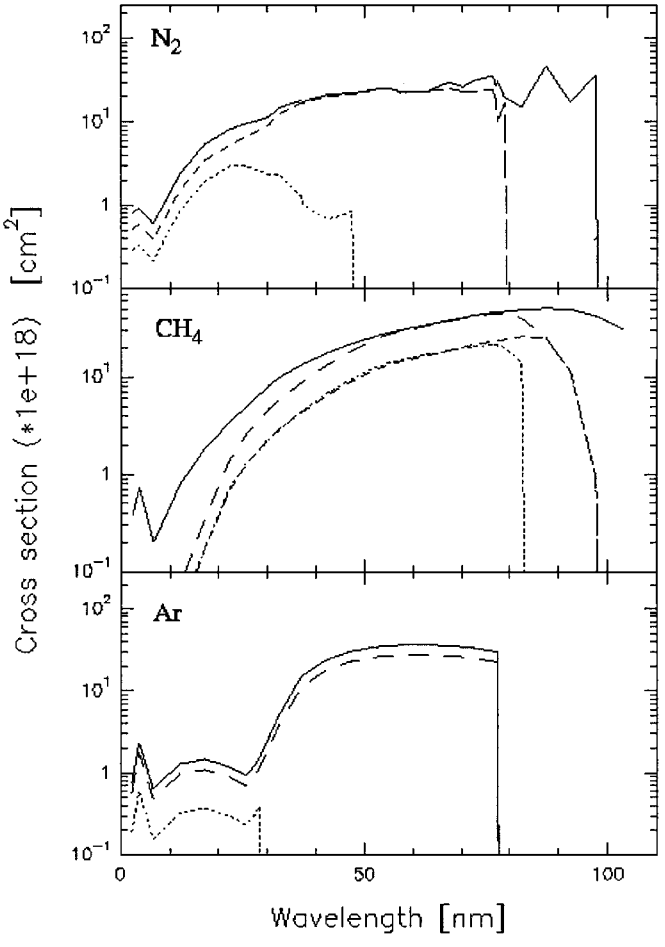

FIG. 2. The photoabsorption cross sections for N_2 (Torr and Torr 1985, Fennelly and Torr 1992), CH_4 (Samson *et al*. 1989), and Ar (Berkowitz 1979, Marr and West 1976) in Titan's upper atmosphere. The solid lines are for the total absorption cross sections, which include the total ionization cross sections (long-dashed line), divided in the nondissociative (medium-dash line), and dissociative or double ionization (small-dash line) cross sections.

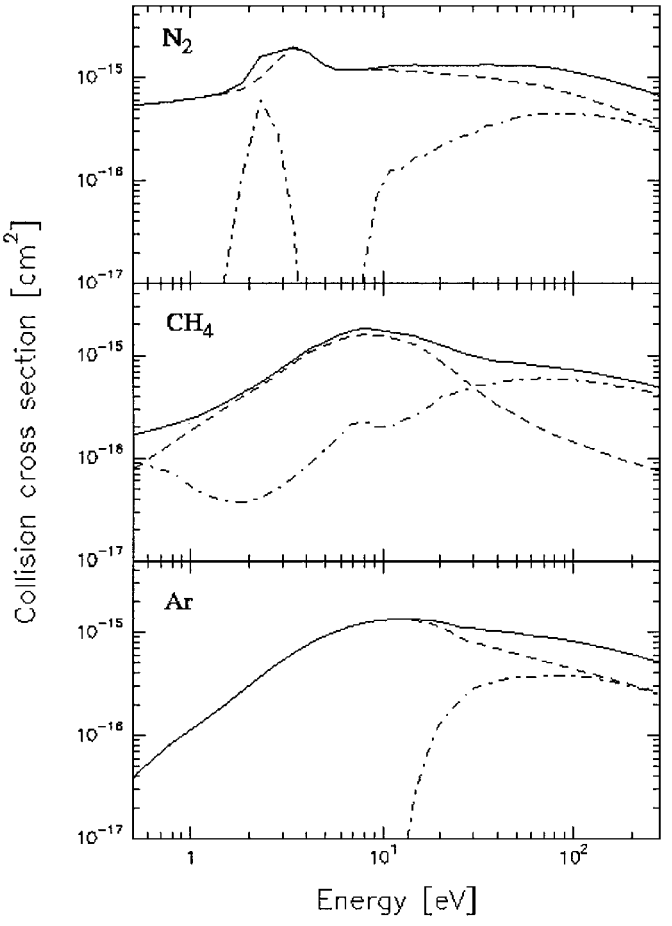

FIG. 3. The collision cross sections for electron impact with N_2 (Lummerzheim and Lilensten 1994), CH_4 (Davies *et al*. 1989), and Ar (Bretagne *et al*. 1986). The solid line represents the total collision cross sections, which include the elastic (dashed line) and the inelastic (dashed-dotted line) cross sections.

3. FIRST CASE: THE DIURNAL IONOSPHERE

For this case, Titan is located in the interplanetary medium, the only energy source being the solar EUV; the model is applied near the equator. The solar EUV flux is interpolated in terms of decametric index, from measurements obtained from the Atmosphere Explorer satellites during solar minimum and maximum conditions (Hinteregger 1981, Hinteregger *et al*. 1981). The values used are those parametrized and modified by Torr and Torr (1985) into 37 energy values from 248 down to 12.02 eV, that is from 5 up to 103 nm (17 discrete solar EUV lines and 20 energy intervals, with averaged fluxes). Following Tobiska (1993), two values have been added at 2.327 and 3.750 nm to take into account ionization due to high energetic photons. The $f_{10.7}$ values used in our simulation correspond to the ones that prevailed during the Voyager 1 encounter of Titan: $f_{10.7} = 256$ with a 3-month average value of 211 (Keller *et al*. 1992). The resulting photon flux is shown in Fig. 4.

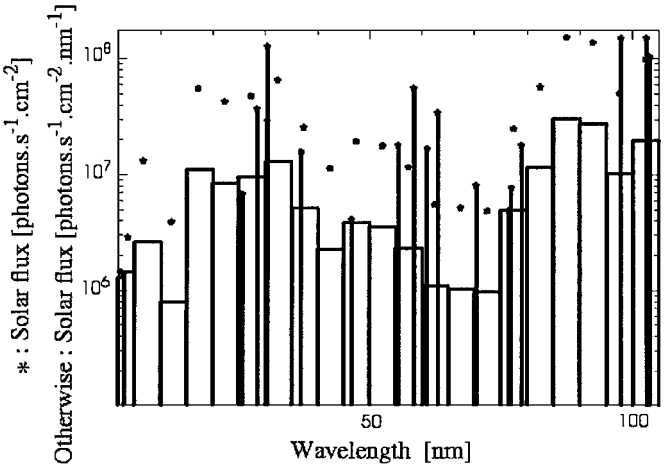

FIG. 4. Solar photon flux shown in 39 wavelength intervals or lines in photons cm^{-2} s^{-1} nm^{-1}; the stars represent the integrated values in units of photons cm^{-2} s^{-1} (Torr and Torr 1987, Tobiska 1993). The solar flux values refer to the location of Titan (≈10 AU).

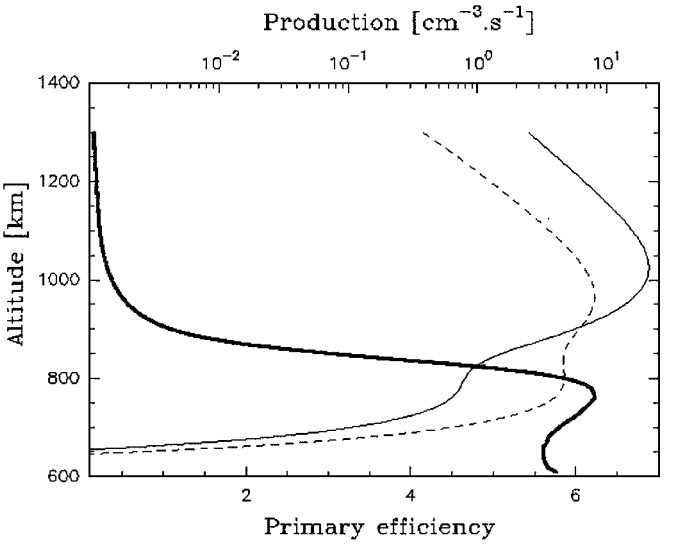

FIG. 6. Primary efficiency (bold line, referring to lower axis) and primary (full line)/secondary (dashed line) electron productions referring to the upper axis.

3.1. The Ion Production

Following Lebonnois and Toublanc (1999), we have taken a solar zenith angle of 45°. The computed ion production rates, deduced from (4) and (5), are shown in Fig. 5. The total electron production rate integrated over the altitude is equal to 7.0×10^8 cm^{-2} s^{-1}. The electron production profile exhibits an F-like region with a maximum around 1000 km, and an E-like region peaking around 750 km, two regions produced by the solar photons and the electrons produced. In the former region, the primary production is larger than the secondary one by a factor of about 6 (only 3 at Earth). In the latter however, the secondary production becomes preponderant. The electron production peaks from about 4 (in the E-like region) to 25 (in the F-like region) electrons s^{-1} cm^{-3}, much less than the thousands in Earth's ionosphere, in accordance with the facts that the distance from Titan to the Sun is 10 times larger and that the atmospheric environments (species, optical depth, ...) are different.

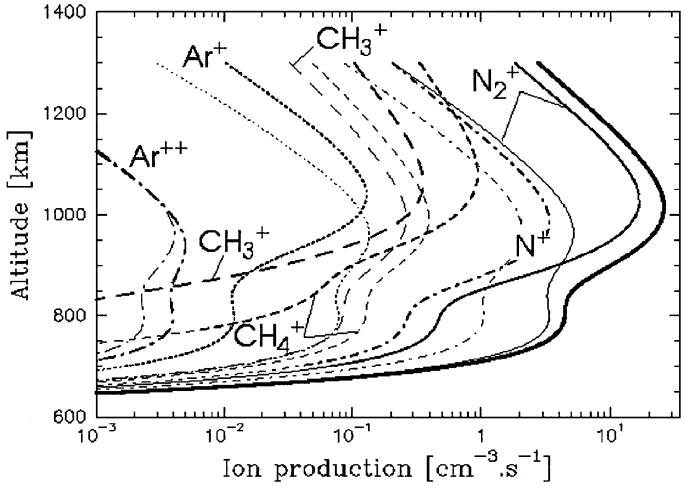

FIG. 5. Ion productions computed for the diurnal case, with solar zenith angle equal to 45°. The bold lines are for the primary production. The thin lines show the secondary production. The thick solid line represents the total electron production.

Figure 6 shows the ratio of the secondary production over the primary production (or primary efficiency) versus altitude. Similar ratios between primaries and secondaries are observed in Earth's ionosphere and have been described by Richards and Torr (1988) and Lilensten *et al.* (1989). They have proven to be dependent on the solar activity level. However, a reason for this dependence is the change of the terrestrial neutral atmosphere under different activity levels. The change of Titan's atmosphere is not known for the moment, and it is therefore not possible to study the change of the primary efficiency under different solar conditions. We checked that changing only the solar input flux (for a constant atmosphere) keeps the efficiency approximately constant, although the productions vary. Therefore, the efficiency plotted in Fig. 6 can be used to infer a rough estimate of the secondary production from the computation of the primary production (solely due to photoionization).

Finally, Fig. 7 shows in color plate the evolution of the total electron production rate versus the solar zenith angle. The computation is valid for the same conditions as defined in the beginning of Section 3, that is near the equator, for a solar activity $f_{10.7}$ of 256 with a 3-month average value of 211. Not surprisingly, the altitude for the maximum increases when the Sun sets, going from about 1000 km at a solar angle of 5° to 1150 km for a solar angle of 85°. The production rate (with the active solar conditions described above) is less than 2 cm^{-3} s^{-1}.

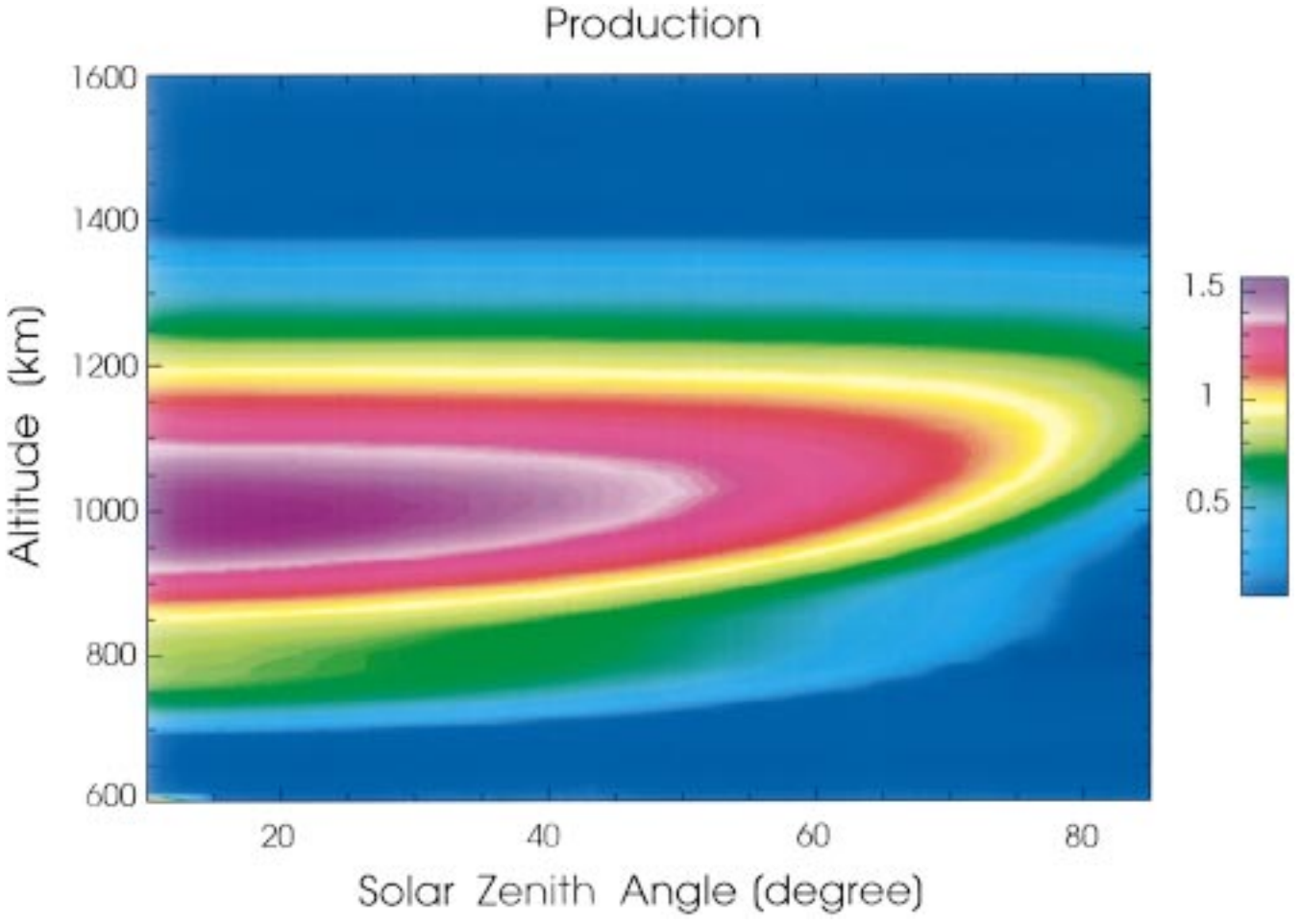

FIG. 7. Total electron production in cm^{-3} s^{-1} as a function of altitude and solar zenith angle.

3.2. The Electron Density

3.2.1. The chemical model. In order to compute the electron density we have combined the photochemical model of Toublanc *et al*. (1995) and the ionosphere model of Keller *et al*. (1992). We will not describe here in detail those two models. Starting with the neutral photochemical model of Toublanc *et al*. (1995), four primary reactions involving nitrogen, methane, and electrons are added in the chemical scheme. The dissociation and ionization of these compounds in the thermosphere as the result of interactions with energetic photons and electrons produce $N(^4S)$, N_2^+, N^+, CH_4^+, and CH_3^+ (see Fig. 5). These productions are included in the model as a net altitude dependent production for these atoms and ions. We have then included the chemical scheme described in Keller *et al*. (1992). We should note that the neutral or ion chemistry is driven by the dissociation or ionization of nitrogen and methane. We have made our computations with a solar zenith angle of 45°, the continuity equation is then solved for each species from the surface up to 1600 km. Secondary electrons are produced when primary electrons ionize nitrogen or methane. These electrons are not very energetic and they more or less recombine rapidly with ions. Previous models have shown that the major ion is H_2CN^+ or heavy hydrocarbon ions. We should, however, note that H_2CN^+ could react with some other heavy hydrocarbons or nitriles to produce long chains: H_2CN^+ may not be the major ion, confirming the conclusion found by Fox and Yelle (1997). We do not follow all these heavy ions generically called Z^+. There is also a recombination of these heavy ions with electrons giving back neutral heavy molecules. Our model also takes into account the formation of aerosols; their production rates have been estimated around 10^{-14} g cm^{-2} s^{-1} (e.g., Rannou *et al*. 1995). Keller *et al*. (1992) have two important recombination reactions involving these species and estimated a rate. As our model showed, the electron density is mainly sensitive to the Z^+ recombination and depending upon the rate this density could vary in a large range. As Voyager I gave an upper limit of ionospheric electron density, we can adjust the rate so that the density is lower that what was measured. Having in mind all these problems which need further studies we have, however, attempted to compute a distribution of electrons. This model also reproduced the mixing ratio of all major hydrocarbons and the size, distribution, number

density, and production rate of the aerosols. The reactions associated with the neutral (photo)chemistry and their rates used in this study are given and discussed in Table III of Toublanc *et al.* (1995) and in Tables I and II of Lara *et al.* (1996). The ion-neutral reactions and their rates can be found in Table III of Keller *et al.* (1992). Note that recently Keller *et al.* (1998) proposed newly kinetic rates. The details of the calculations will be presented in a future paper.

3.2.2. Density results. The ion density results are presented in Figs. 8a to 8e and the electron density in Fig. 9. The total ion (or electron) density exhibits a familiar Earth shape profile.

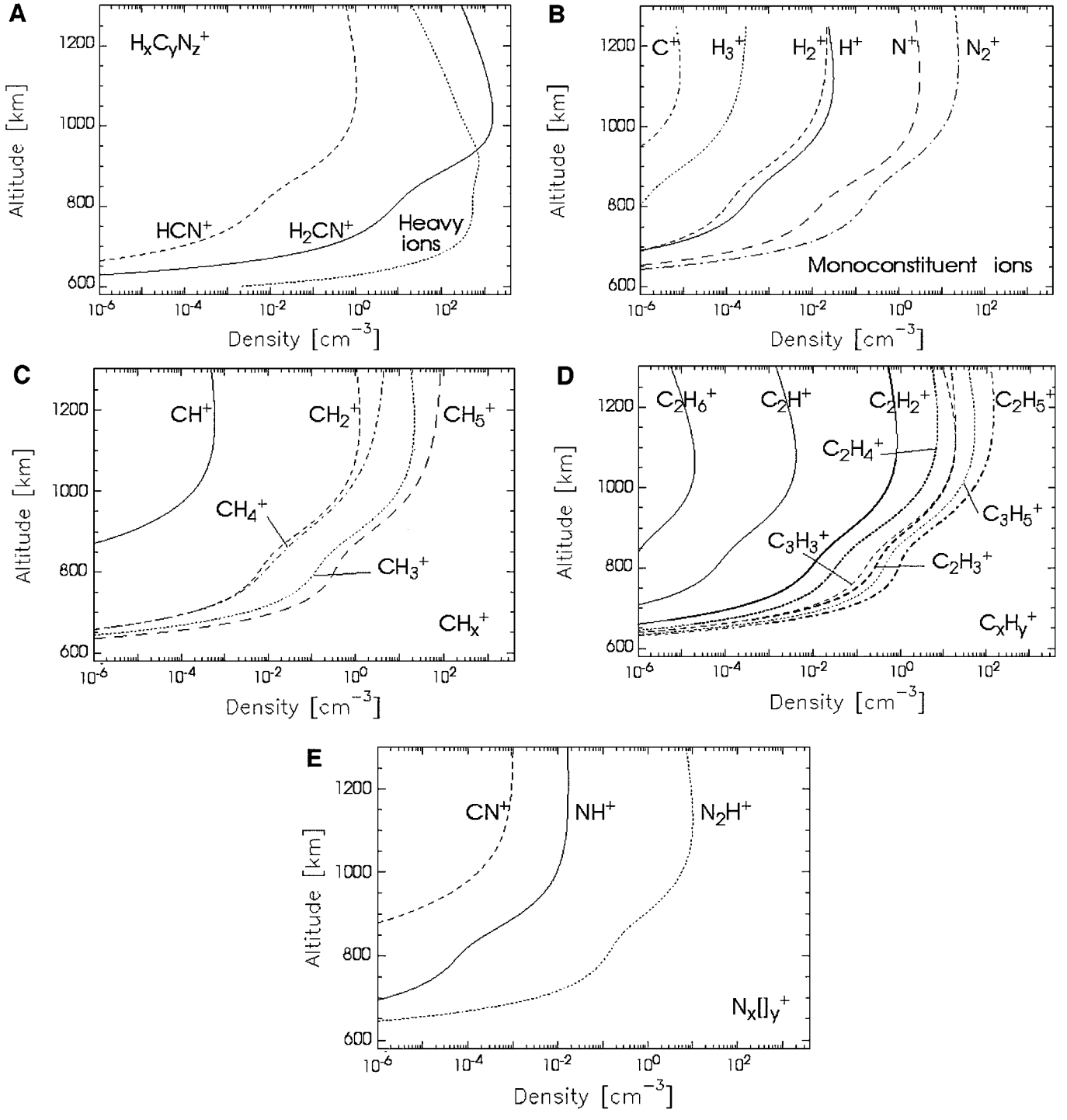

FIG. 8. (a–e) Ion densities plotted on the same scale for the different ion species. The "heavy ions" refer to the group called Z^+ in the text.

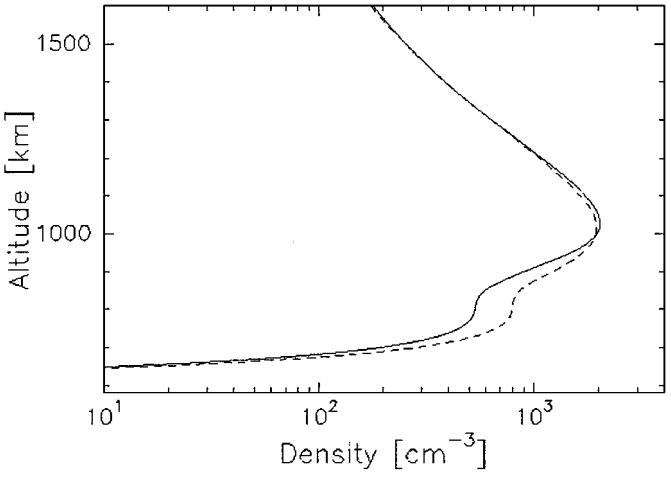

FIG. 9. The full line shows the electron density computed from a comprehensive chemical code. The dashed line is the approximation computed from a recombination coefficient method.

Moreover, it is close to that in Keller *et al*. (1992), at least in the shape of the height profile. The maximum in electron density is reached at a height of about 1050 km in both approaches. Even though those two studies have been performed for two different solar zenith angles (45° here and 60° there), Fig. 7 shows that this change has only a slight effect on the altitude of the maximum production. As for comparison with observations, the height of the peak electron density computed is in agreement with Voyager 1 data: an altitude between 900 and 1100 km was derived from the radio occultation measurements during egress (morning terminator) (Lindal *et al*. 1983) and an altitude of 1180 ± 150 km was obtained for ingress (evening terminator) (Bird *et al*. 1997). It should be noted that, even though the observations are associated with day/night terminator, "the upper ionospheric heights sounded by the radio signal at egress would have been subjected to ionization by solar EUV radiation for about two days prior to the occultation" and "the atmospheric layers at 1000 km altitude [sounded by the radio signal at ingress] would not have been shadowed by the limb for almost two days" (Bird *et al*. 1997).

The electron density profile we obtain reaches a maximum of about 2×10^3 electrons per cubic centimeter. Keller *et al*. (1992) found a value 50% greater than ours. This could be explained by the differences in the cross sections and reaction rates. An upper limit of 5×10^3 electrons cm^{-3} during egress (Lindal *et al*. 1983) and a maximum of $2.4 \times 10^3 \pm 1.1 \times 10^3$ electrons cm^{-3} during ingress (Bird *et al*. 1997) have been deduced from observations: they are of the order of our computation value.

Concerning the ion compositions, the fact that we introduced a sink for H_2CN^+ leads to a larger density of the heavy ions Z^+ (see Fig. 8a). A test of our chemical model lies in the comparison of the aerosol distribution and density inferred from Voyager observations. A microphysics code is included in our program in order to produce aerosols by coalescing and condensing heavy molecules. Photochemistry and ionochemistry are then responsible for the net production of these heavy molecules. The total amount of aerosols produced this way is roughly 10^{-14} g cm^{-2} s^{-1} which is the value currently admitted by several authors (Rannou *et al*. 1995). This part will be further described in a future paper.

3.2.3. Effective coefficient calculation. The determination of the electron density from the electron production requires a comprehensive chemistry code. A simple approach consists in considering that the only recombination phenomenon is the recombination between N_2^+ and electrons. The stationary chemical equation leads to

$$N_e = \sqrt{\frac{P(z)}{\alpha_{\text{eff}}}}, \tag{6}$$

where $P(z)$ refers to the total electron production (sum of the primary and the secondary ones) and α_{eff} to the effective recombination coefficient (Oran *et al*. 1981). In our case, this coefficient reduces to the chemical reaction rate ζ of the recombination between N_2^+ and electrons. This coefficient depends on the electron temperature: $\zeta = \frac{6.06 \times 10^{-6}}{\sqrt{T_e}}$ in cm^3 s^{-1}. In order to take into account the complex real chemical scheme of the ionosphere of Titan, we let our effective recombination coefficient be a multiple of this recombination rate: $\alpha_{\text{eff}} = a \cdot \zeta$.

This method gives very good results in the terrestrial E region and can give only a rough idea of what to expect in Titan's ionosphere. Due to the lack of data, the electron temperature is taken equal to the neutral temperature. Were the electron temperature twice as large as the neutral temperature, the result would be multiplied only by 0.71, which would not much change our estimate.

With this simple approach, we find that $a = 15$, or in other words:

$$N_{\text{e}} = \sqrt{\frac{P(z)}{15 \times \frac{6.06 \times 10^{-6}}{\sqrt{T_{\text{e}}}}}}. \tag{7}$$

The height profile of the estimated electron density (dashed line, Fig. 9) is very close to the height profile computed with the comprehensive chemical code, above the maximum of the F-like region (solid line, Fig. 9). At lower altitude, there appears a slight discrepancy. One could compute an altitude dependent correction factor a, but to the present stage of our knowledge of the neutral atmosphere in Titan, this would be a useless computation. Instead, this simple formula (7) makes it possible to compute a rough estimate of the electron density from the total electron production. In addition, it should be recalled that the total electron production may be deduced from the primary electron production through (3) and (4) and from the secondary electron production determined in applying the primary efficiency, plotted in Fig. 6, to the primary production.

3.3. The Nitrogen Emission Intensities and Comparisons with Observations

Another output of the transport equation is the excitation rate. Equation (5) can be applied, with the excitation cross sections in place of the ionization ones. Many of the excited ions and atoms return to equilibrium via the emission of electromagnetic waves. As far as N_2^+ is concerned, the Meinel band (640–800 nm) is due to the deexcitation of the $A^2\Pi_u$ state. The first negative band (391.4 nm and 427.8 nm) comes from the deexcitation of the $B^2\Sigma_u^+$ state. For predissociative states, the state $c_4'^1\Sigma_u^+ - X^1\Sigma_g^+$ lead to the c_4' Rydberg band (with (0,0) at 95.8 nm, (0,1) at 98.1 nm, (0,2) at 100.3 nm, (3,0) at 90.4 nm, (3,2) at 94.4 nm, (3,3) at 96.4 nm, and (4,0) at 88.7 nm), and the state $b_1'\Sigma_u^+$ to NII (63–109 nm). Both of them may emit in the NI (85.5–149.3 nm) range. The excitation and dissociative excitation states lead to the second positive band (320–380 nm), the first positive (red–IR), the Vegard–Kaplan (340–378 nm), the LBH (127.3–210 nm), and the BH (95–170 nm) bands and some others of smaller intensity (Watson–Koontz, Janin, Gaydon–Herman bands).

Some of those emissions have been measured by the Voyager 1 ultraviolet spectrometer (UVS) (Broadfoot *et al*. 1981). By the time of the observation, Titan was exposed to the sunlight, but also to Kronian particle precipitations, which are not taken into account in this section. Up to now, a comparison with the unique observations by Voyager 1 is certainly the only way to validate our computation. The results are shown in Table I, with intensities in Rayleigh; in the first column the type of nitrogen emission lines or bands is specified. The second column shows the measured intensities (disk averaged) as published in Strobel and Shemansky (1982) and Strobel *et al*. (1991) with new calibration of the UVS for some of the emissions. "Error bars on bright spectral features of ±50% would not seem unreasonable," as quoted from Strobel *et al*. (1992). The third column of Table I displays our results, using the neutral atmosphere plotted in Fig. 1. The excited atoms are due both to photoexcitation and to collision excitation with secondary electrons. The agreement between observations and computation is reasonable when considering the omission of the particle precipitations and all the uncertainties on the actual solar flux and those on the composition of the atmosphere.

TABLE I
Intensities in Rayleigh of Nitrogen Emissions

Type	Voyager 1 UVS	With Ar	Without Ar	$f_{<25.7\text{nm}} * 2$	$f_{<25.7\text{nm}}/2$
391.4 nm		21.6	21.7	43.2	10.8
427.8 nm		6.7	6.8	13.4	3.3
Meinel		118.7	118.7	237.3	59.3
Second positive		31.6	31.7	63.1	15.8
First positive		71.3	71.7	142.7	35.7
Vegard–Kaplan		190.8	291.0	381.7	95.4
LBH	96[a,b]	69.6	70.0	139.1	34.8
BH	15.2[b]–25.3[a]	25.5	25.7	51.0	12.7
N I	77.5[a]	45.0	45.3	89.9	22.5
N II	8.6[b]–14.4[a]	4.8	4.8	9.6	2.4
Rydberg	24.1[b]–40.2[a]	38.8	39.1	77.6	19.4

[a] Strobel and Shemansky 1982.
[b] Strobel *et al.* 1991, new calibration of the UVS.

To estimate the influence of the atmospheric model, the N_2 density is increased or reduced by a factor of two at all altitude levels: the nitrogen emission intensities undergo changes lower than 8%. However, significant variations on emission intensities occur when the uncertainties of the solar flux are taken into account. For wavelengths smaller than 25.7 nm, a fudge factor of 2 or $\frac{1}{2}$ can be applied to the photon flux. Even though the physical process is not linear, the response is almost linear; the resulting intensities are increased or reduced by the same factor 2 (see columns 5 and 6 of Table I and compare with column 3). Moreover these extreme values of the nitrogen intensities, taking into consideration the uncertainties of the photon solar flux, enclose the measured values obtained from Voyager.

A similar computation was performed by Gan *et al*. (1992) with a two-stream simulation. Their cross sections are slightly different from ours. They used a solar index of 256, with the reference spectrum *SC*#21*REFW* (Hintereger *et al*. 1981): in order to compare with their results, we have chosen the same solar flux in our computations. Their study includes the effect of magnetospheric electron precipitations. Since this effect accounts for a few percent in their results, we compare our computations without precipitations. The two computed LBH band intensities are close to each other (65 *R* in Gan *et al*. (1992), 69.6 *R* in the present work), and far from the observations (96 *R*). BH band proposed by Gan *et al*. (1992) is 81 *R*, much larger than ours (25.5 *R*) and than that observed (15–25 *R*). The NI line in Gan *et al*. (1992) concerns three states and is 4.0 *R*. For the same states, the observation is 45.9 *R*. Our estimate for all states is 45 *R*, also smaller than the observed value (77.5 *R*). Finally, the Rydberg value for $c_4'(0, 0)$ is 26 *R* (Gan *et al*. 1992). The observation for this only state is 8 *R*. The observation for all states is in the 24- to 40-*R* range. Our computed value is 38.8 *R*. One difference between the two computations (except for the two/multistream approach) is that Gan *et al*. (1992) do not take into account photodissociative excitation of N_2, but this is not sufficient to explain the discrepancies. Both transport codes have been widely tested under different conditions, so that to this point, we can only see here an effect of the different cross section sets used.

There is a debate going on the presence of argon in Titan's ionosphere after the nondetection of its resonance lines (Strobel *et al*. 1992 and references therein). Strobel *et al*. (1992) constructed four different models of atmosphere (with different mixing ratios of CH_4 and Ar) and then compared the relative intensities of the Ar resonance lines with a N^+ multiplet; this comparison makes it possible to evaluate the upper limit of the argon abundance in Titan's atmosphere: the Ar mixing ratio is limited to 0.1 at the tropopause. Here we check if it would be

possible to evaluate the presence of argon using the nitrogen emissions computed above. Indeed, the emissions are intense enough so that one could expect to observe them from an Earth-orbiting spacecraft. In Table I, column 4 shows the estimation of these emissions (in Rayleigh) without argon in the neutral model. This percentage varies from 0 to 1.3%. Therefore, this method does not make it possible to conclude from the observation of the nitrogen emission spectra on the presence of argon in Titan's atmosphere.

4. SECOND CASE: THE NOCTURNAL IONOSPHERE

This second case deals with Titan inside Saturn's magnetosphere. The study is applied to polar regions on the nightside: the considered source of energy is the Kronian electron precipitations. Our understanding of the magnetic field geometry in the vicinity of Titan is mainly based on Voyager 1 observations (Ness *et al*. 1982, Kivelson and Russel 1983): Titan's ionosphere created initially by photoionization interacts directly with the flow of charged particles trapped in Saturn's magnetosphere. The ionospheric plasma loads the incident flow, slows it down, and causes the field lines to drape around Titan. This interaction is extremely complex as shown by Neubauer *et al*. (1984) and, to our knowledge, has not been modeled in a usable form. The main issue for our purpose is the knowledge of the form of the field lines when they penetrate the ionosphere, which depends on the thermal ionospheric pressure. When the ionosphere is produced by electron impacts only, it is weak enough that it merely disturbs the field lines (Keller *et al*. 1994). Therefore, for simplicity, we assume that the field lines are perpendicular to the satellite at its poles, as shown in Fig. 10.

4.1. The Precipitated Electron Flux

The electron precipitations that are considered in our model come from the Voyager measurements. Voyager 1 and 2 entered the magnetosphere of Saturn in the early afternoon local time and exited in the dawn hemisphere, about two days later. Titan was the prime target of Voyager 1's encounter and the magnetic shell crossing occurred inbound at magnetic latitude $\lambda \approx 0.1^\circ$, whereas the standoff distance of the magnetopause—which is the distance from the magnetopause to the planet in the solar direction—was at $R_{\rm sub} = 24\ R_{\rm s}$ (Behannon *et al*. 1983). Using a three-dimensional model of Saturn's magnetosphere (Maurice and Engle 1995), we estimate the outbound Titan magnetic shell crossing at $z \approx 6\ R_{\rm s}$ (altitude above the equatorial plane) and $\lambda \approx 18^\circ$. The Voyager 1 encounter took place under quiescent conditions in the outer magnetosphere, but Voyager 2 found highly disturbed conditions. For Voyager 2, the standoff distance of the magnetopause was $R_{\rm sub} = 19\ R_{\rm s}$ (Behannon *et al.* 1983) inbound; therefore, Titan's orbit was in the magnetosheath. During the outbound path, the standoff distance was varying around $R_{\rm sub} = 40\ R_{\rm s}$. Using the 3D model of Saturn's magnetosphere, we estimate an average magnetic crossing for Voyager 2 outbound at $z \approx -9\ R_{\rm s}$ and $\lambda \approx -30^\circ$.

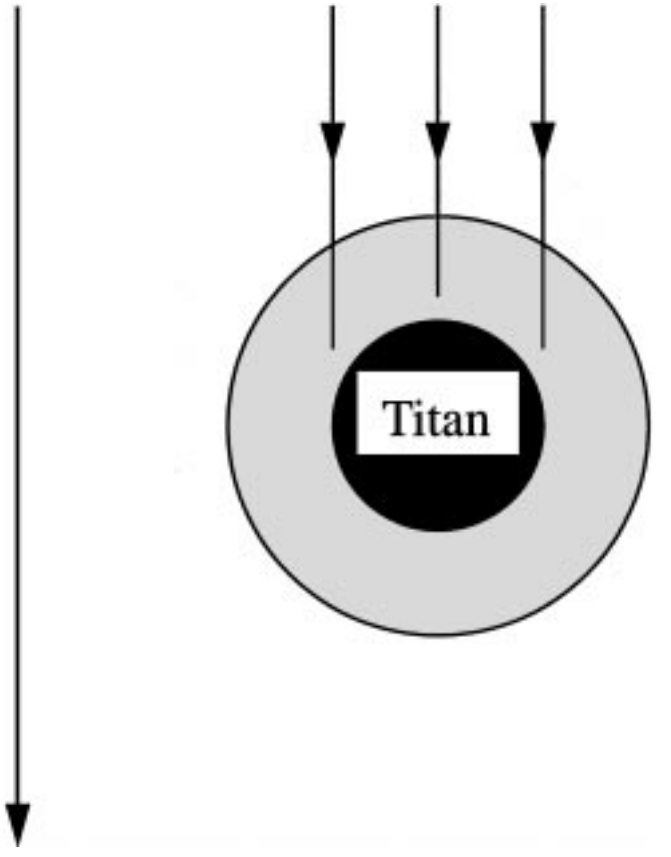

FIG. 10. The simple model of magnetic field used in this study, that is vertical filed line at the poles.

Two instruments onboard the Voyagers have measured electron fluxes near Titan's orbit. The plasma science (PLS) experiment (Sittler *et al*. 1983) has covered the 10 eV to 6 keV energy range. However, the signal above about 1 keV was frequently below the detection level of the instrument. The low energy charged particle (LECP) experiment (Krimigis *et al*. 1983) made measurements from 20 to 200 keV on Voyager 1, and from 20 keV to 1 MeV on Voyager 2. Maurice *et al.* (1996) have gathered these data sets on a unique 15-min time scale inside 18.5 $R_{\rm s}$. Figure 11 is a continuation of this work at 20 $R_{\rm s}$. From 10 eV to 1 MeV (with a large data gap between 1 and 20 keV), the electron fluxes, in $\mathrm{cm^{-2}\ s^{-1}\ keV^{-1}\ sr^{-1}}$, extend over eight orders of magnitudes. On this figure all the measured electron fluxes at Titan (Voyager 1 and Voyager 2, inbound and outbound) fall into the shaded area.

Measurements at Titan magnetic shell crossings span over about one order of magnitude. The reasons of this dispersion are a lack of accuracy of the magnetic field model which is used to detect the Titan shell crossings, the time variability of the trapped electron populations in Saturn's outer magnetosphere, and the latitudinal effects. We model a mean electron flux precipitating on Titan by a single kappa isotropic distribution: $\Phi(E, \mu) = 6 \times 10^8 E(1+17E)^{-2.9}$ in $\mathrm{cm^{-2}\ s^{-1}\ keV^{-1}\ sr^{-1}}$, where $\Phi(E, \mu)$ is the electron precipitated flux with E, the energy in keV and

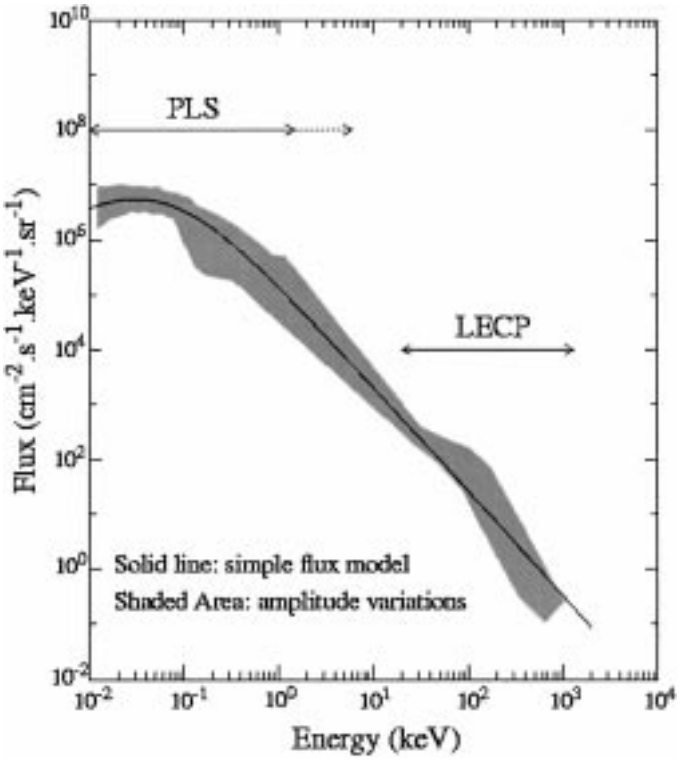

FIG. 11. Electron observations at Saturn when crossing Titan's magnetic shell. Measurements by the PLS (10 eV to 6 keV) and LECP (20 keV to 1 MeV) instruments are gathered for Voyager 1 and 2 inbound (in) and outbound (out) paths. Data were log-log extrapolated across the energy gap. A simple kappa distribution function is used to model the mean flux (see text).

μ, the cosine of the pitch angle. This distribution is overplotted in Fig. 11.

4.2. The Stationary Electron Flux and Ion Production Rate

Using this precipitating electron flux as an input (i.e., source function of (1)), Fig. 12 displays the computed stationary electron flux in Titan's ionosphere at four different altitudes. The fluxes have been integrated in angle over each hemisphere and projected perpendicularly to the magnetic field (taken vertical, above one pole), providing the total flux; they are given as a function of particle energy (cm^{-2} s^{-1} eV^{-1}),

$$\text{flux}(z, E) = 2\pi \left| \int_0^1 d\mu \cdot \mu \cdot \Phi(z, E, \mu) \right| + 2\pi \left| \int_{-1}^0 d\mu \cdot \mu \cdot \Phi(z, E, \mu) \right|,$$

where z represents the altitude and Φ the stationary electron flux computed from (1). As they propagate in Titan's ionosphere, the electrons degrade their initial energy in many inelastic scattering processes, among which ionization and predissociative ionization. Through the values of associated cross sections, the different collisional processes contribute to the structure of the curves: for example, the dip between 2 and 4 eV is caused by the excitation of vibrational levels in N_2 (Rees 1989 and references therein). The ion and electron production rates are deduced from this stationary electron flux and shown in Fig. 13. The ionization cross sections being of about the same magnitude for the 3 neutral species, the different ion production rates follow the same order as the neutrals in density. The electron production rate is then mostly due to the ionization of the dominant neutral species, that is nitrogen; it peaks at 650 km with a value of about 2 electrons s^{-1} cm^{-3}.

The uncertainties and the variability of the precipitated flux modeled in Section 4.1 hardly exceed an order of magnitude (Maurice *et al.* 1996). Therefore, we estimate the maximum excursion that the electron production rate may have, by multiplying or dividing the Voyager electron flux by 10. Such an operation leads to a variation of the production rate by about the same factor of 10 above 600 km. Another way to estimate a frame for the electron production rate in Titan's ionosphere is to compute it using maximum and minimum measured input fluxes. This computation is shown in Fig. 14 in addition with

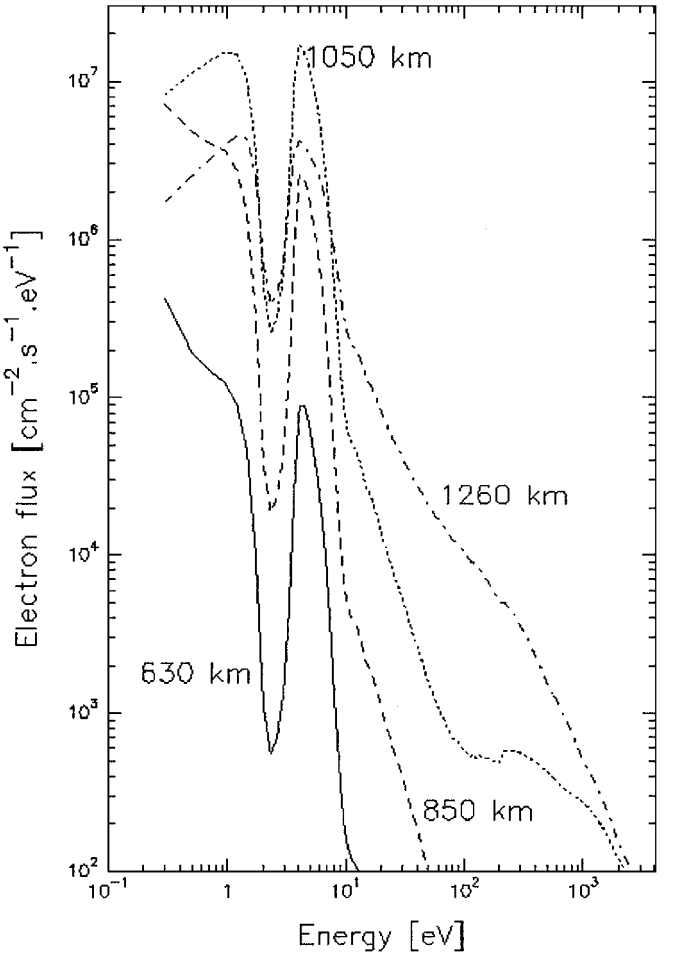

FIG. 12. Total projected electron fluxes at different altitudes. The computation was performed on 16 angles and 200 energies. The altitude of the incident flux is 1300 km.

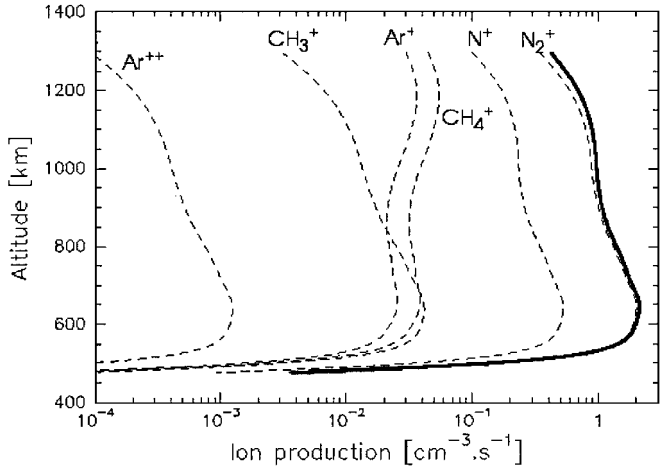

FIG. 13. Ion production computed for the nocturnal case. The thick solid line represents the total electron production. As no photoelectrons are produced, no primary production is generated.

the electron production rate previously discussed. The use of a precipitating flux made out of the upper border of the shaded area in Fig. 11 leads to a production rate peaking at about 550 km with a value of about 5 electrons s^{-1} cm^{-3}. When the input flux is the minimum one, made from the lower border of the shaded area in Fig. 11, we find a maximum production rate of 1 to 2 electrons s^{-1} cm^{-3}.

5. SUMMARY AND DISCUSSION

We have computed the electron and ion production rates at Titan for two different configurations. For the diurnal equatorial conditions, with Titan outside Saturn's magnetosphere, the gross properties of Titan's ionosphere are similar to those of Earth's with E- and F-like regions. We have compared the primary and secondary electron production rates: the deduced primary efficiency is not significantly dependent on the zenith angle if the neutral atmosphere is assumed constant. This efficiency can be used to deduce the secondary electron production from the primary one which can be easily computed from (3) and (4). Moreover, we have proposed an effective recombination coefficient by comparison of the electron density computed from a comprehensive chemical model and a simple recombination approach. Such a coefficient makes it possible to easily compute the electron density profile from the total electron production rate with a reasonable accuracy. We have also shown that the analysis of nitrogen emission spectra does not provide any constraint on the presence of argon in Titan's atmosphere.

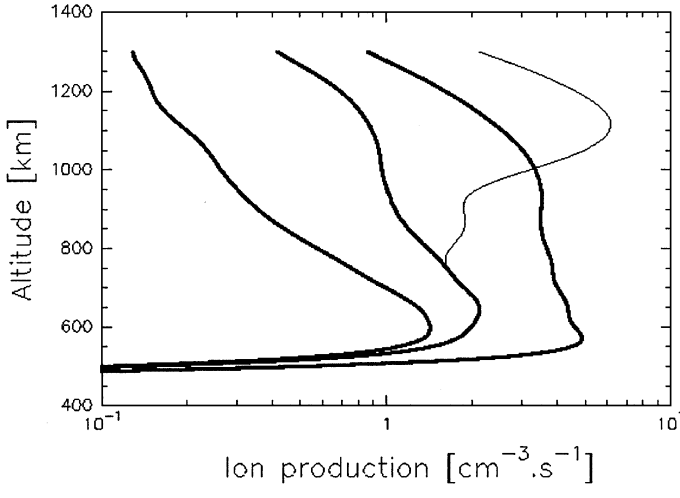

FIG. 14. The total ion production for three precipitating electron fluxes in the nocturnal case; the fluxes are (from left to right) a flux made from the minimum border of the shaded area in Fig. 11, the kappa model, the upper border. The thin line shows the expected additional electron production due to the superimposition of photoionization at solar angle of 64°.

We have performed a comparison with the UVS measurements of nitrogen emission spectra from Voyager 1 observations. This comparison is twofold. (1) The calculated N_2 emission intensities are consistent with the UVS observations (detailed in Section 3.3). Although Voyager 1 was inside the Kronian magnetosphere during these measurements, we cannot conclude that the electron precipitations have no effect on Titan's ionosphere structure. The emissions we present are indeed primarily due to photoexcitations. Uncertainties on the input parameters (solar flux, neutral atmosphere, cross sections) may hide the (minor) contribution of the electron precipitation to these emissions. (2) With a comprehensive chemical model, we have computed a maximum electron density of 2×10^3 electrons cm^{-3}, peaking around 1000 km. An upper limit of 5×10^3 electrons cm^{-3} between 900 and 1100 km was derived from the Voyager 1 radio occultation measurements during egress (morning terminator) (Lindal *et al*. 1983). The ingress data associated with evening terminator have been reexamined by Bird *et al*. (1997): they are consistent with a maximum electron density of $2.4 \times 10^3 \pm 1.1 \times 10^3$ electrons cm^{-3} at an altitude of 1180 ± 150 km. Therefore values between computations and observations are consistent.

For the nocturnal polar conditions, we present the degradation of precipitating electrons in Titan's atmosphere and the associated ion production. The incident flux was modeled by a kappa distribution from all Voyager measurements near Titan magnetic shell. This nocturnal case study is very prospective and offers no immediate validation. We have adopted a crude approximation for the field line geometry. The "vertical field model" is strictly valid for the brief period of time when Titan is in Saturn's shadow (5h40 per 16 days when the ring inclination is $<2.9°$); this duration is expected to be much larger than the lifetime of H_2CN^+, usually the major and last ion constituent of Titan's ionosphere. At other times, this geometry gives an upper limit of the contribution of the precipitating electrons to the formation of the ionosphere, since the ionization is maximum under the normal incidence. Other authors have used other field representations applying to the wakeside of Titan (Gan *et al*. 1992, Keller *et al*. 1994). The originality of our study is that it makes use of precipitating electron fluxes as measured at Titan.

The total ion production in the diurnal case is, at its maximum, about one order of magnitude larger than the production in the nocturnal case (see Figs. 5 and 13). Keeping in mind the restrictions we have set on the magnetic field geometry, we superimpose a EUV photon flux to the electron precipitation at Titan's pole. We use a solar zenith angle of 64° which is the minimum one at Titan's poles; this leads to a maximum value for the vertical component of total photon energy flux of 3.8×10^{-3} erg cm^{-2} s^{-1}. Our model of the electron precipitation gives 6×10^{-3} erg cm^{-2} s^{-1}. Figure 14 displays the additional ion production due to the UV light. As expected, this production is very effective between 1000 and 1200 km. It drops below 800 km because of the large solar angle, where the production due to the precipitating electrons becomes dominant.

Evidently, future developments of this work must include a better definition of the field lines draped around Titan and the precipitations of Kronian ions as an extra ionization source. Theoretical studies of the interaction between Titan and the Kronian magnetic field are going on in several places (Cravens *et al.* 1998, Ledvina and Cravens 1998, Kabin *et al.* 1999). Moreover, in the vicinity of Titan, ion species are probably N^+ and H^+, which may interact with Titan's atmosphere. Nevertheless, a realistic description of the proton or ion penetration path in Titan's ionosphere is not easily feasible: the ions are fast enough that their gyroradii are roughly the size of Titan (Cravens *et al*. 1992).

ACKNOWLEDGMENTS

We thank D. Strobel and A. Coustenis for helpful discussions. We are very indebted to J. Bretagne for providing us with a wonderful set of argon cross sections and to E. Lellouch for initiating us to the neutral atmosphere of Titan. We thank E. Lellouch, as well as W. Kofman, for useful discussions and for a careful reading of the manuscript. We also thank A. Richmond for helpful comments. Part of the computations presented in this paper were performed at the Centre de Calcul Intensif de l'Observatoire de Grenoble. M.G. gratefully acknowledges the financial support of the Advanced Study Program and the High Altitude Observatory, divisions of the National Center for Atmospheric Research (NCAR). NCAR is sponsored by the National Science Fondation.

REFERENCES

Barret, J. L., and P. B. Hays 1976. Spatial distribution of energy deposited in nitrogen by electrons. *J. Chem. Phys.* **64**, 743–750.

Behannon, K. W., R. P. Lepping, and N. F. Ness 1983. Structure and dynamics of Saturn's outer magnetosphere and boundary regions. *J. Geophys. Res.* **88**, 8791–8800.

Berkowitz, J. 1979. *Photoabsorption, Photoionization and Photoelectron Spectrometry*. Academic Press, New York.

Bird, M. K., R. Dutta-Roy, S. W. Asmar, and T. A. Rebold 1997. Detection of Titan's ionosphere from Voyager 1 Radio occultation observations. *Icarus* **130**, 426–436.

Blelly, P.-L., J. Lilensten, A. Robineau, J. Fontanari, and D. Alkaydé 1996. Calibration of a numerical ionospheric model using EISCAT data: Effect of the neutral atmosphere and the suprathermal electrons on the ionospheric plasma structure. *Ann. Geophys.* **14**, 1375–1390.

Bretagne, J., G. Callude, M. Legentil, and V. Puech 1986. Relativistic electron-beam-produced plasma. I. Collision cross sections and loss function in argon. *J. Phys. D* **19**, 761–780.

Broadfoot, A. L., and 15 colleagues 1981. Extreme ultraviolet observations from Voyager 1. *Science* **212**, 206–211.

Cravens, T. E., C. N. Keller, and L. Gan 1992. The ionosphere of Titan and its interactions with saturnian magnetospheric electrons. In *Proceedings, Symposium on Titan*, Toulouse, September 9–12, 1991, ESA SP-338, pp. 273–278.

Cravens, T. E., C. J. Lindgren, and S. A. Ledvina 1998. A two-dimensional multifluid MHD model of Titan's plasma environment. *Planet. Space Sci.* **46**, 1193–1205.

Davies, D. K., L. E. Kline, and W. E. Bies 1989. Measurements of swarm parameters and derived electrons collision cross sections in methane. *J. Appl. Phys.* **65**, 3311–3323.

Fennelly, J. A., and D. G. Torr 1992. Photoionization and photoabsorption cross sections of O, N2, O2, and N for aeronomic calculations. *At. Data Nucl. Data Tables* **51**, 321–363.

Fox, J. L., and R. V. Yelle 1997. Hydrocarbon ions in the ionosphere of Titan. *Geophys. Res. Lett.* **24**, 2179–2182.

Gan, L., C. N. Keller, and T. E. Cravens 1992. Electrons in the ionosphere of Titan. *J. Geophys. Res.* **97**, 12137–12151.

Hall, D. T., D. E. Shemansky, and T. M. Tripp 1992. A reanalysis of Voyager UVS observations of Titan. In *Proceedings, Symposium on Titan*, Toulouse, September 9–12, 1991, ESA SP-338, pp. 69–74.

Hinteregger, H. E. 1981. Representation of solar EUV fluxes for aeronomical applications. *Adv. Space Res.* **1**, 39–52.

Hinteregger, H. E., K. Fukui, and B. R. Gilson 1981. Observational, reference and model data on solar EUV, from measurements on AE-E. *Geophys. Res. Lett.* **8**, 1147–1150.

Kabin, K., T. I. Gombosi, D. L. De Zeeuw, K. G. Powell, and P. L. Israelevich 1999. Interaction of the saturnian magnetosphere with Titan: Results of a three-dimensional MHD simulation. *J. Geophys. Res.* **104**, 2451–2458, 1999.

Keller, C. N., V. G. Anicich, and T. E. Cravens 1998. Model of Titan's ionosphere with detailed hydrocarbon ion chemistry. *Planet. Space Sci.* **46**, 1157–1174.

Keller, C. N., T. E. Cravens, and L. Gan 1992. A model of the ionosphere of Titan. *J. Geophys. Res.* **97**, 12117–12135.

Keller, C. N., T. E. Cravens, and L. Gan 1994. One-dimensional multispecies magnetohydrodynamic models of the ramside ionosphere of Titan. *J. Geophys. Res.* **99**, 6511–6525.

Kivelson, M. G., and C. T. Russell 1983. The interaction of flowing plasmas with planetary ionospheres: A Titan–Venus comparison. *J. Geophys. Res.* **88**, 49–57.

Krimigis, S. M., J. F. Carbary, E. P. Keath, T. P. Armstrong, L. J. Lanzerotti, and G. Gloeckler 1983. General characteristics of hot plasma and energetic particles in the saturnian magnetosphere: Results from the Voyager spacecraft. *J. Geophys. Res.* **88**, 8871–8892.

Lara, L. M., E. Lellouch, J. J. Lopez-Moreno, and R. Rodrigo 1996. Vertical distribution of Titan's atmospheric neutral constituents. *J. Geophys. Res.* **101**, 23261–23283.

Lebonnois, S., and D. Toublanc 1999. Actinic fluxes in Titan's atmosphere from 1D to 3D. Application to high latitude composition. *J. Geophys. Res.*, submitted.

Ledvina, S. A., and T. E. Cravens 1998. A three-dimensional MHD model of plasma flow around Titan. *Planet. Space Sci.* **46**, 1175–1191.

Lilensten, J., P-L. Blelly, W. Kofman, and D. Alcaydé 1996. Auroral ionospheric conductivities: A comparison between experiment and modeling, and theoretical $f_{10.7}$ dependent model for EISCAT and ESR. *Ann. Geophys.* **14**, 1297–1304.

Lilensten, J., W. Kofman, J. Wisemberg, E. S. Oran, and C.R. DeVore 1989. Ionization efficiency due to primary and secondary photoelectrons: A numerical model. *Ann. Geophys.* **7**, 83–90.

Lindal, G. F., G. E. Wood, H. B. Hotz, D. N. Sweetnam, V. R. Eshleman, and G.L. Tyler 1983. The atmosphere of Titan: An analysis of the Voyager 1 radio occultation measurements. *Icarus* **53**, 348–363.

Lummerzheim, D., and J. Lilensten 1994. Electron transport and energy degradation in the ionosphere: Evaluation of the numerical solution. Comparison with laboratory experiments and auroral observations. *Ann. Geophys.* **12**, 1039–1051.

Lummerzheim, D., M. H. Rees, and H. R. Anderson 1989. Angular dependent transport of auroral electrons in the upper atmosphere. *Planet. Space Sci.* **37**, 109–129.

Mantas, G. P. 1973. *Electron Collision Processes in the Ionosphere*. Aeronomy Report 54. Aeronomy Laboratory, Dept. of Electrical Engineering, Univ. of Illinois, Urbana, IL.

Marr, G. V., and J. B. West 1976. Photoionization cross sections. *At. Data Nucl. Data Tables* **18**, 497–508.

Maurice, S., and I. M. Engle 1995. Idealized Saturn magnetosphere shape and field. *J. Geophys. Res.* **100**, 17143–17151.

Maurice, S., E. C. Sittler, J. F. Cooper, B. H. Mauk, M. Blanc, and R. S. Selesnick 1996. Comprehensive analysis of electron observations at Saturn: Voyager 1 and 2. *J. Geophys. Res.* **101**, 15211–15232.

Ness, N. F., M. H. Acuna, K. W. Behannon, and F. M. Neubauer 1982. The induced magnetosphere of Titan. *J. Geophys. Res.* **87**, 1369–1381.

Neubauer, F. M., D. A. Gurnett, J. D. Scudder, and R. E. Hartle 1984. Titan's magnetospheric interaction. *Saturn* 760–787.

Nilsson, H., S. Kirkwood, J. Lilensten, and M. Galand 1996. Enhanced incoherent scatter plasma lines. *Ann. Geophys.* **14**, 1462–1472.

Oran, E. S., and D. J. Strickland 1978. Photoelectron flux in the Earth's ionosphere. *Planet. Space Sci.* **26**, 1161–1177.

Oran, E. S., V. B. Wickward, W. Kofman, and A. Newman 1981. Auroral plasma lines: A first comparison of theory and experiment. *J. Geophys. Res.* **86**, 199–205.

Rannou, P., M. Cabane, E. Chassefiere, R. Botet, C. P. McKay, and R. Courtin 1995. Titan's geometric albedo: Role of the fractal structure of the aerosols. *Icarus* **118**, 355–373.

Rees, M. H. 1989. *Physics and Chemistry of the Upper Atmosphere*, Cambridge Atmospheric and Space Science Series, Cambridge Univ. Press, Cambridge.

Richards, P. G., and D. G. Torr 1988. Ratio of photoelectron to EUV ionization rate for aeronomic studies. *J. Geophys. Res.* **93**, 4060–4066.

Samson, J. A. R., G. N. Haddad, T. Masuoka, P. N. Pareek, and D. A. L. Kilcoyne 1989. Ionization yields, total absorption and dissociative photoionization cross sections of CH_4 from 110–950 Å. *J. Chem. Phys.* **90**, 6925–6932.

Sittler, E. C. Jr., K. W. Ogilvie, and J. D. Scudder 1983. Survey of low-energy plasma electrons in Saturn's magnetosphere. *J. Geophys. Res.* **88**, 8847–8870.

Stamnes, K. 1981. On the two-stream approach to electron transport and thermalization. *J. Geophys. Res.* **86**, 2405–2410.

Stamnes, K., and M. H. Rees 1983. Inelastic scattering effects on photoelectron spectra and ionospheric electron temperature. *J. Geophys. Res.* **88**, 6301–6309.

Strobel, D. F., and D. E. Shemansky 1982. EUV emission from Titan's upper atmosphere: Voyager 1 encounter. *J. Geophys. Res.* **87**, 1361–1368.

Strobel, D. F., R. R. Meier, and D. J. Strickland 1991. Nitrogen airglow sources: Comparison of Triton, Titan and Earth. *Geophys. Res. Lett.* **18**, 689–692.

Strobel, D. F., M. E. Summers, and X. Zhu 1992. Titan's upper atmosphere: Structure and ultraviolet emissions. *Icarus* **100**, 512–526.

Tobiska, W. K. 1993. Recent solar extreme ultraviolet irradiance observations and modelling: A review. *J. Geophys. Res.* **98**, 18879–18893.

Torr, M. R., and D. J. Torr 1985. Ionization frequencies for solar cycle 21: Revised. *J. Geophys. Res.* **90**, 6675–6678.

Toublanc, D., J. P. Parisot, J. Brillet, D. Gautier, F. Raulin, and C. P. McKay 1995. Photochemical modelling of Titan's atmosphere. *Icarus* **113**, 2–26.

Wolf, D. A., and F. M. Neubauer 1982. Titan's highly variable plasma environment. *J. Geophys. Res.* **87**, 881–885.

Yelle, R. V., D. F. Strobel, E. Lellouch, and D. Gautier 1997. Engineering models for Titan's atmosphere. In *Huygens: Science, Payload and Mission*. (E. Wilson, Ed.), ESA SP-1177. Noordwijk, The Netherlands.